Hindawi
Geofluids
Volume 2023, Article ID 2361703, 9 pages
https://doi.org/10.1155/2023/2361703

Research Article

Research on Microscopic Pore Structure Characteristics and Producibility of the Chang 9 Reservoir in the Wucangpu Block

Bin Shi, Fangping Chen, Hailong Dang, Zili Jia, Binchi Hou, Lihua Shi, Shengsong Kang, and Tao Wang

Research Institute of Shaanxi Yanchang Petroleum (Group) Co., Ltd, Xi'an, Shaanxi 710065, China

Correspondence should be addressed to Bin Shi; 161002211@stu.cuz.edu.cn

Received 12 October 2022; Revised 16 November 2022; Accepted 22 March 2023; Published 16 May 2023

Academic Editor: Ming Wen

The pore structure can affect the storage and flow properties of rock, which is an important research content in the study of unconventional tight reservoirs. This research hopes to clarify the reservoir characteristics and fluid seepage mechanism of the Chang 9 reservoir in the Wucangpu block and provide technical support for the development of horizontal wells with staged fracturing in this block. In this paper, the microscopic pore structure characteristics and producibility of the reservoir in the study area are analyzed in detail by means of constant-rate mercury intrusion and nuclear magnetic resonance. The research results show that the reservoir with permeability less than 0.076 mD is mainly composed of microthroat, the reservoir with permeability of 0.208-0.633 mD has a larger proportion of microthin throat, and the reservoir with permeability of 2.722-3.998 mD has a larger proportion of fine-middle throats. The results show that the oil/gas in the rock sample reservoirs with permeability greater than 1.0 mD is easy to produce.

1. Introduction

With the major breakthroughs in shale oil exploration and development in North America, tight oil has become a hot spot in the world's unconventional oil and gas exploration and development [1–3]. The sandstone reservoir with a low matrix permeability is called a low (extralow) permeability reservoir. It is an unconventional reservoir formed after various types of rocks are subjected to a certain degree of secondary transformation. Compared with conventional reservoirs, tight oil reservoirs are more complex macroscopically and microscopically. In addition to their fine particle size and poor physical properties, their heterogeneity is particularly prominent [4–9]. The heterogeneity is mainly manifested in differences in lithology, physical properties, seepage capacity, and diagenetic evolution in tight reservoirs. Tight oil reservoirs generally have the characteristics of fine particle size and high hetero base, and the lithology mainly includes sandstone, siltstone, sandy carbonate rock, limestone, and dolomite [10].

Different from conventional oil and gas reservoirs, tight oil reservoirs are dominated by nano- and microscale pore throats and develop multiscale and multitype pores. Many types of pores constitute the effective storage space of tight oil. Reservoir micropore structure research technology and characterization methods are important means to solve oil and gas exploration and development; especially with the deepening of conventional and unconventional oil and gas reservoir micropore structure research, reservoir lithology is diverse, pore structure is complex and diverse, and the characteristics of fluid seepage are complex. Conventional methods such as ordinary thin sections [11, 12], scanning electron microscopes [13], image grain analysis [14], particle size analysis, and high-pressure mercury intrusion [15] are often used as basic projects in the research of pore structure, which can be used to characterize the shape and structure of pores. Nowadays, constant-rate mercury intrusion, nuclear magnetic resonance, and other methods can further conduct more precise quantitative research on pores, distinguish pores and roars, and divide movable fluid boundaries. In this

paper, the microscopic pore structure characteristics and playability analysis of low-/ultra-low-permeability reservoirs in the study block are given by means of constant-rate mercury intrusion and nuclear magnetic resonance.

2. Methods and Theory

2.1. Geological Background. The Wucangbao oilfield is located in the middle section of the Yi-Shaan slope, which is the broadest part of the Ordos Basin. The overall performance is a west-dipping monoclinic with a gradient of only about 1° and an average slope of 6-8 m/km. The north of the area is adjacent to the Xin'an border area of Dingbian Oil Production Plant, and the east and west sides are surrounded by the Changqing Oilfield operation area. The total area of the work area is 402 km^2 [16, 17]. The Chang 9_1 sandstone formation in the Wucangpu block generally belongs to the delta front facies deposits. The 6 coring wells in the east are located in the main part of the underwater distributary channel, and the 2 coring wells in the west are located on the flanks of the underwater distributary channel. The sand body in the main part of the channel is thick, and the sorting is good while the sand body flanking the channel is thin and the sorting is poor. This is consistent with the oil-bearing grade and core physical property analysis results displayed by well logging. The locations of the coring wells are shown in Figure 1. The cores of this project are taken from 40 cores from six coring wells in Chang 9 oil layer in Wucangpu block.

2.2. Constant-Speed Mercury Intrusion. Constant-speed mercury intrusion refers to the method of mercury injection at a constant and low speed [18, 19]. In the quasistatic process, the microstructure of the pore is determined according to the natural pressure fluctuation of the meniscus at the mercury injection end when it passes through microscopic pores of different shapes. It can be assumed that the interfacial tension and contact angle remain unchanged during the mercury injection process. When the mercury passes through the pore throat into the wider pore body, the mercury pressure drops suddenly. The quasistatic mercury injection process ensures that the pressure change only corresponds to the change of the radius of curvature of the meniscus of mercury, that is, the change of the capillary pressure, so that the fluctuation of the pressure is controlled by the throat and pores of the reservoir. When the pore passes through the throat and enters the next pore, it corresponds to the process of pressure drop, rise, and fall. The maximum mercury injection pressure used in the constant-speed mercury intrusion experiment is 900 psi (100 psi = 0.6895 MPa), and the corresponding throat radius is about 0.12 μm. Usually, we refer to the throat and controlled pores with a radius of less than 0.12 μm as ineffective throats and ineffective pores in the seepage process [19, 20]. The parameters that can be derived from the constant velocity mercury intrusion mainly includes the following:

(1) Microscopic homogeneity coefficient (α) [21]: defined as the total deviation of each throat radius from the largest throat radius. The larger the value of α, the closer the throat radius of the constituent sample is to the maximum throat radius, and the more uniform the throat distribution of the sample is, where α_i is the normalized distribution frequency density for each throat radius

$$a = \frac{(\sum r_i \alpha_i)}{r_{\max}}. \tag{1}$$

(2) Average throat radius: defined as the root mean square of the throat radius distribution

$$\overline{R_c} = \sqrt{\left(\sum_{i=1}^{n} r_i^2 \alpha_i\right)}. \tag{2}$$

(3) Contribution of a single throat to permeability:

$$\Delta K_i = \frac{r_i^2 \alpha_i}{\sum r_i^2 \alpha_i}. \tag{3}$$

(4) Relative sorting coefficient: it is the variance of the throat radius divided by the average radius. The smaller the relative sorting coefficient, the more concentrated the throat size distribution is on the average, and the more uniform the pore structure is. δ is the variance

$$\mathrm{CCR} = \frac{\delta}{\overline{R_c}}, \tag{4}$$

$$\delta = \sqrt{\sum \left(r_i - \overline{R_c}\right)^2 \alpha_i}. \tag{5}$$

2.3. NMR. NMR is the interaction between atomic nuclei and a magnetic field. Since water is rich in hydrogen nucleus 1H, the most used atomic nucleus in natural gas exploration and development research is hydrogen nucleus 1H [22, 23]. After the rock sample is saturated with water, due to the nuclear magnetic moment of the hydrogen nuclei in the water, the nuclear magnetic moment will produce energy level splitting in the applied static magnetic field. The nuclear magnetic resonance phenomenon can be observed by appropriate detection and receiving coils, and the nuclear magnetic resonance signal (magnetization vector) can be detected. The nuclear magnetic resonance signal intensity is proportional to the number of hydrogen nuclei contained in the measured sample. For pure material samples (such as pure water), the surrounding environment of each hydrogen nucleus and the interaction of the nuclei are the same; thus, the relaxation time T2 can be used to describe the physical properties of the sample. The mineral composition and pore structure in the reservoir rock are very complex. For rock porous medium samples, the situation is much more complicated. The fluid exists in the porous medium and is surrounded by many interfaces. The inconsistency of the

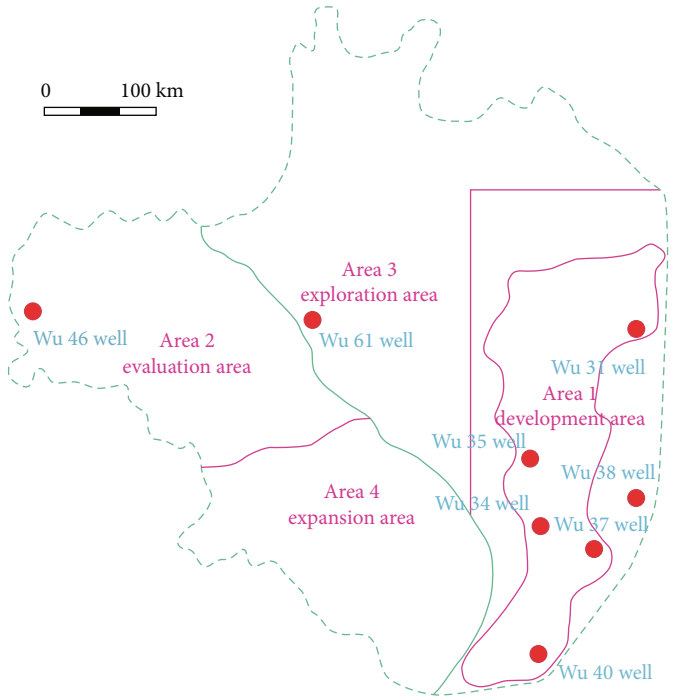

Figure 1: Location map of coring well.

contact opportunities of paramagnetic impurities on the surface makes the probability of each nuclei to be enhanced different. Thus, the nucleus relaxation in the rock-fluid system cannot be described by a single relaxation time but should be a distribution. The physical properties of different rock-fluid systems determine that they have different T_2 distributions, so their physical properties can be determined by obtaining their T_2 distributions in turn.

According to the fast diffusion surface relaxation model of nuclear magnetic resonance, the nuclear relaxation in a single channel can be described by a relaxation time. At this time, T_2 can be expressed as

$$\frac{1}{T_2} = \frac{1}{T_{2B}} + \rho_2 \frac{S}{V} + \frac{\gamma^2 G^2 D \tau^2}{3}, \tag{6}$$

where the first term on the right is called the bulk relaxation term, the size of T_{2B} depends on the properties of the saturated fluid, which can be removed, and the third term on the right is called the diffusion relaxation term. By using the established NMR dediffusion measurement experiment technology, the third item can also be removed. After removing the first and third terms on the right, formula (6) becomes

$$\frac{1}{T_2} = \rho_2 \frac{S}{V}, \tag{7}$$

where r_2 is the surface relaxation strength, which depends on the pore surface properties and mineral composition, and S/V is the specific surface area of a single pore, which is inversely proportional to the pore radius.

For rock porous media composed of pores of different sizes, the total relaxation is the superposition of the relaxation of a single pore (the relaxation of a single pore is expressed by formulas (2)–(6)), namely,

$$S(t) = \sum A_i \exp\left(\frac{-t}{T_{2i}}\right), \tag{8}$$

where $S(t)$ is the total NMR signal intensity and A_i is the proportion of the relaxation time T_{2i} component, that is, the percentage of the pore volume of a certain pore size corresponding to T_{2i} to the total pore volume.

The basic data collected by NMR T_2 measurement is the echo train, that is, the decay curve of the total nuclear magnetic signal intensity $S(t)$ with time t in the T_2 relaxation process. Multiexponential fitting is performed on the echo train, to obtain the A_i corresponding to each T_{2i}. We take T_{2i} as the abscissa and A_i as the ordinate and then the distribution of the T_2 relaxation time; that is, the T_2 spectrum can be obtained.

T_2 relaxation in rock fluids is much more complicated. In addition to the strengthening of the surface paramagnetic ions (the strengthening method is the same as the T_1 relaxation), the inhomogeneity of the magnetic field inside the system and the molecular diffusion caused the T_2 relaxation to be further strengthened due to the different magnetic permeability of the rock particles and the fluid. At this time, T_2 can be expressed as

$$\frac{1}{T_2} = \rho_2 \frac{S}{V} + \frac{\gamma^2 G^2 D \tau^2}{3}, \tag{9}$$

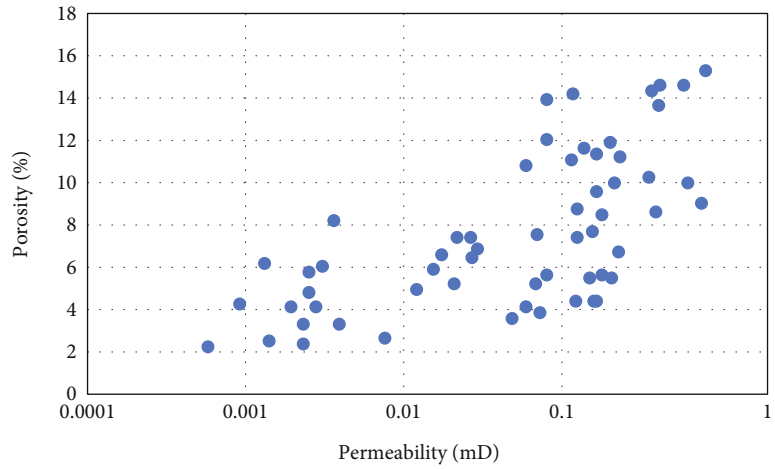

Figure 2: The relationship between core porosity and permeability.

where D is the diffusion coefficient, G is the inhomogeneity of the internal magnetic field, which is proportional to the external magnetic field, and τ is the echo interval. It can be seen from the formula that when the external field is not very strong (corresponding to G is not very large) and τ is short enough, the contribution of the latter term can be ignored, at this time:

$$\frac{1}{T_2} = \rho_2 \frac{S}{V}. \tag{10}$$

Therefore, the distribution of relaxation time reflects the distribution of the specific surface of the rock medium and the strength of the force on the fluid on the inner surface.

3. Results and Discussion

3.1. Pore Structure Analysis. The core permeability distribution of this block is mainly concentrated between 0.01 mD and 1.00 mD. The average permeability is around 0.60 mD, and the average porosity is around 10.54%. The core permeability distribution displayed by fluorescence is 0.001-0.015 mD, and the porosity distribution is 2.0%-8.0%, while the core permeability distribution shown by oil traces is 0.032-3.997 mD, and the porosity distribution is 5.3%-15.5% (Figure 2).

In this project, a total of 7 rock samples from 4 coring wells in the block were tested for mercury injection at a constant rate. As can be seen from Figure 3, the cores with different permeability have little difference in the pore radius distribution, while the throat radius distribution shows much significant difference. The lower the permeability, the more concentrated the throat radius distribution in the low-value area. As the permeability increases, the distribution range expands to the high-value area, but the peak value of the curve decreases. The seepage capacity of the rock sample is mainly restricted by the throat radius.

From Figure 4, the average throat radius, the maximum throat radius, the average pore-throat ratio, and the sorting coefficient all show a good logarithmic relationship with the permeability. The smaller the permeability, the smaller the average throat radius and the maximum throat radius of the reservoir, and the larger the average pore-throat ratio. When the permeability is less than 0.6 mD, the throat radius decreases sharply, while the pore-throat ratio increases sharply. When the permeability is greater than 0.6 mD, the average throat radius is above 1 μm (fine throat level), and the maximum throat radius is 2 μm (medium throat level). The development difficulty is moderate. The smaller the permeability, the smaller the throat sorting coefficient, indicating that the throat distribution tends to be uniform, and its sorting performance becomes better. When the permeability is greater than 0.6 mD, the throat sorting coefficient is maintained at a high value level, and the degree of throat homogeneity is great.

To sum up, reservoirs with permeability below 0.6 mD have small throats and large pore-throat ratio, while reservoirs with permeability greater than 0.6 mD have a larger pore-throat radius. The pore-throat ratio is small, which reduces the difficulty of water injection and reduces the problem of reservoir production.

The throat radius distribution of cores with different permeability grades has its own characteristics. As shown in Table 1, the reservoirs with permeability value of 0.076 mD are almost all microthroat, which is difficult to develop by water injection. The reservoirs with a permeability of 0.208-0.633 mD have a large proportion of microfine throats, and this kind of reservoir has a certain development potential and can be used as the target of water injection. The reservoir with a permeability of 2.722-3.998 mD has a large proportion of medium throats using water injection development, which is not difficult to develop.

3.2. Research on the Mobility of the Fluids. From the test results, the NMR spectra in the Wucangpu area are dominated by single-peak and double-peak forms, indicating that there are two or more pore structure types in the reservoir. As the permeability decreases, the high peak of the T_2 spectrum gradually shifts to the left (low-value area), indicating that as the permeability decreases, there is less and less movable fluid (Figure 5).

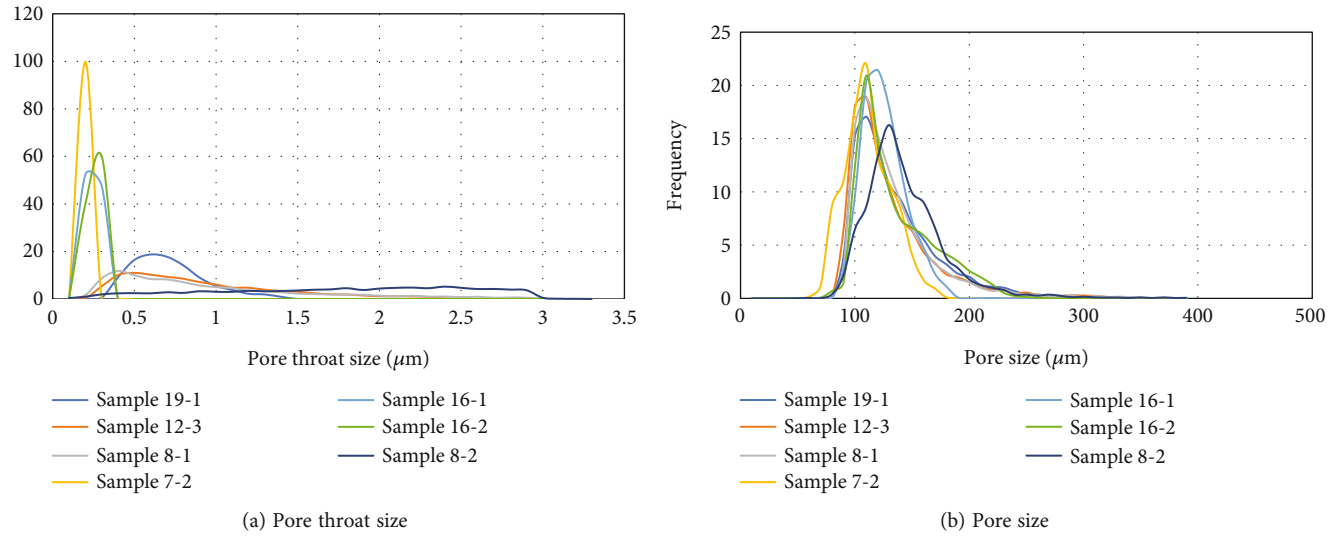

Figure 3: Constant-rate mercury intrusion test results.

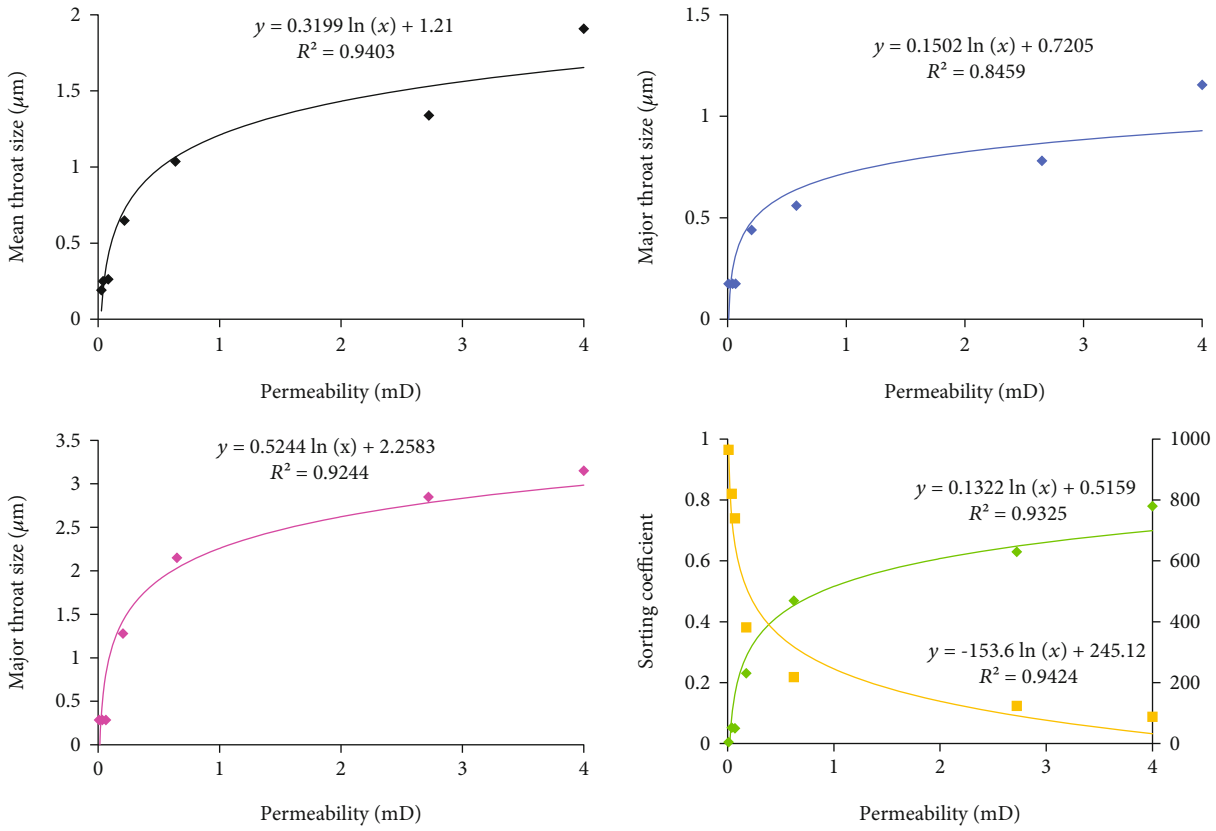

Figure 4: Relationship between throat parameters and permeability.

When the permeability is less than 0.1 mD, as shown in Figure 6, the NMR spectrum mainly appears in the form of a single peak, the fluid is mainly bound fluid, the average movable fluid saturation is 23.68%, and the development potential is small. When the permeability is large, the spectrum curve is elevated in the range of larger relaxation time, and there is a tendency to form a double-peak curve.

When the permeability is greater than 0.1 mD, as shown in Figure 7, the NMR spectrum mainly appears in the form of double peaks. The movable fluid part of the fluid gradually increases with the increase of permeability, and the right front of the spectrum also gradually increases. When the permeability reaches a certain level, the amplitude of the right front is higher than that of the left front, which has

Table 1: Statistics of throat interval distribution.

Core no.	Permeability (mD)	Micro throat ($r \le 0.5\,\mu m$)		Microfine throats ($0.5 < r \le 1\,\mu m$)		Fine throats ($1 < r \le 2\,\mu m$)		Medium throats ($2 < r \le 4\,\mu m$)	
		Proportion (%)	K contribution (%)	Proportion (%)	K contribution (%)	Proportion (%)	K contribution (%)	Proportion (%)	K contribution (%)
8-2	3.998	8.11	0.33	14.03	2.64	37.23	26.61	40.62	70.41
8-1	2.722	32.11	3.99	34.36	16.17	25.39	42.27	8.14	37.57
12-3	0.633	26.73	4.52	41.22	23.80	28.70	56.44	3.35	15.24
19-1	0.208	44.89	19.26	50.12	64.44	4.99	16.30	0.00	0.00
16-2	0.076	100.00	100.00	0.00	0.00	0.00	0.00	0.00	0.00

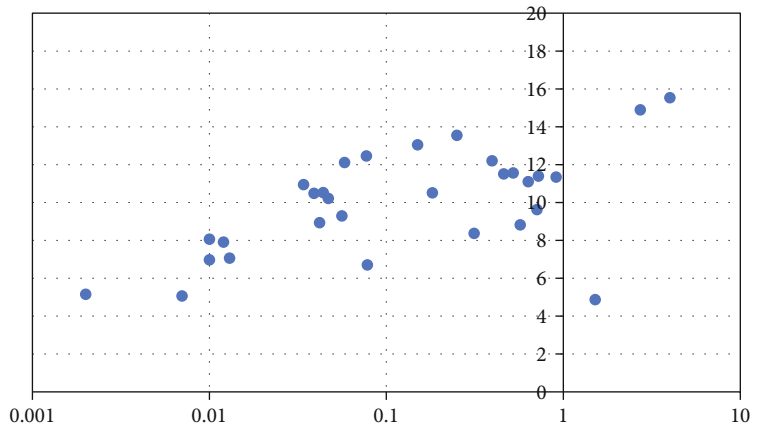

Figure 5: Fluid mobility test results.

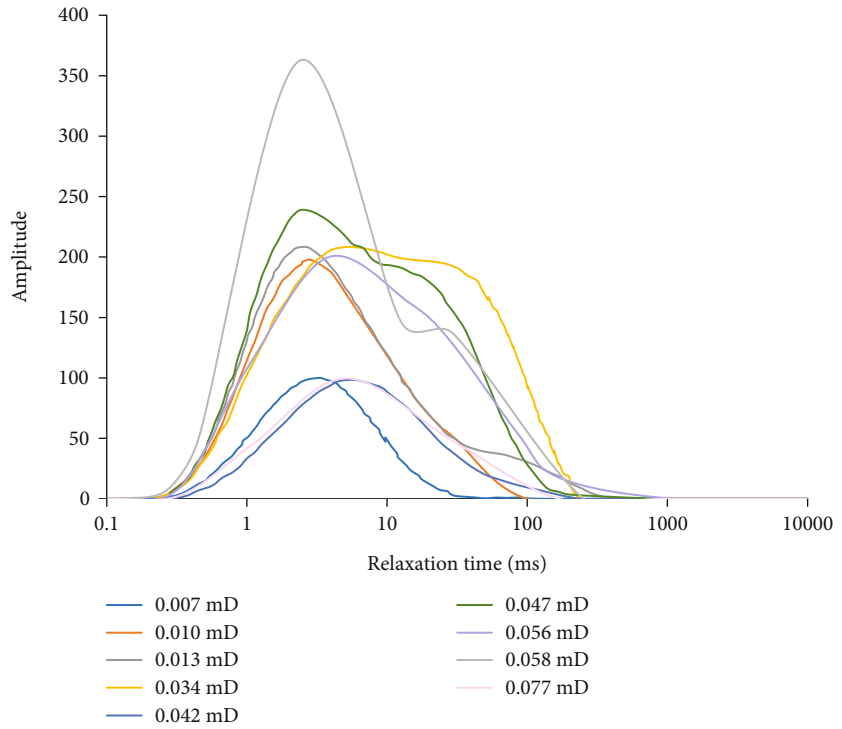

Figure 6: NMR spectra of cores with permeability below 0.1 mD.

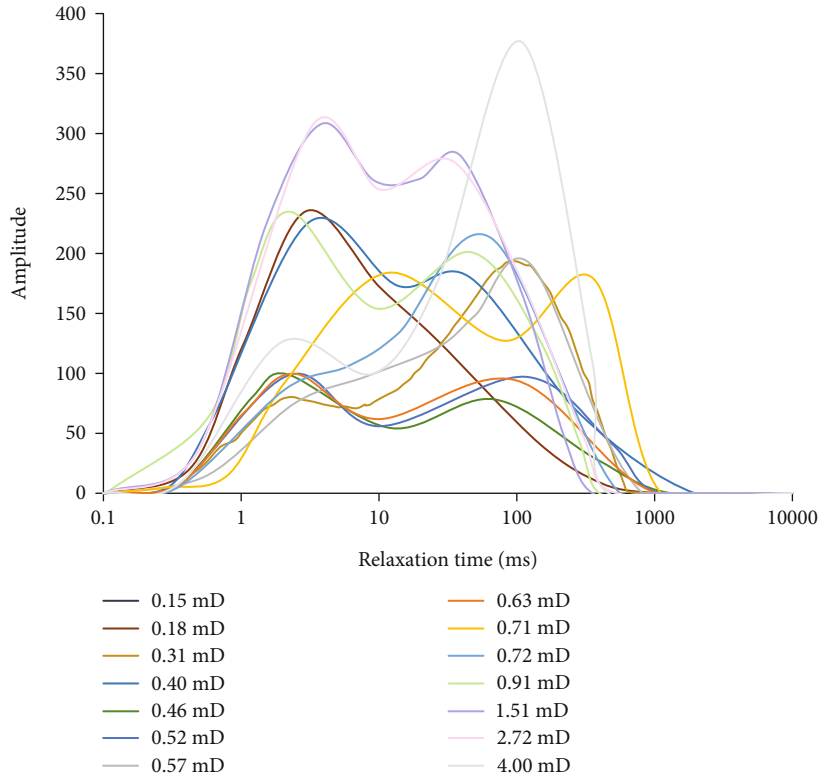

Figure 7: NMR spectra of cores with permeability higher than 0.1 mD.

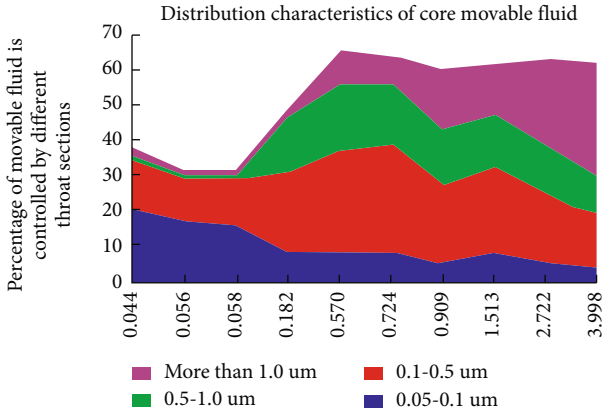

Figure 8: Characteristics of core fluid distribution.

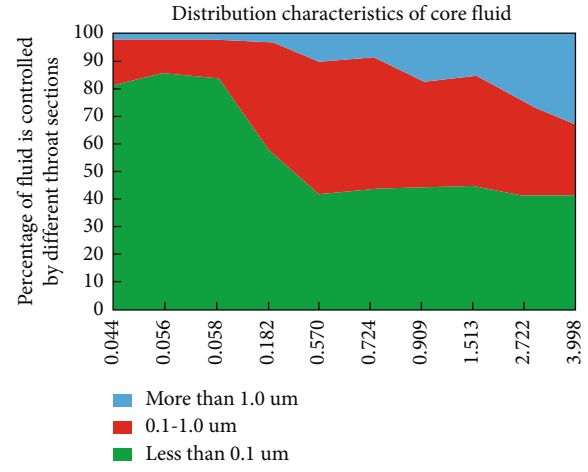

Figure 9: Distribution characteristics of movable core fluid.

great development potential, and the average movable fluid saturation is 55.56%.

The movable fluid saturation increases with the increase of permeability. With the increase of porosity, the movable fluid saturation also shows an upward trend. The average permeability of the Wucangpu block is 0.6 mD, and the corresponding movable fluid saturation is 59.93%. According to the classification evaluation of low-permeability reservoirs, this block belongs to class II reservoirs.

3.3. Research on Fluid Occurrence State. The fluid in the core can be divided into movable fluid and bound fluid. The movable part and the bound part are mainly controlled by the size of the throat. Combined with centrifugal calibration technology, the fluid that can be separated under a certain centrifugal force is called the fluid that can be separated. The dynamic fluid that remains inside the core and cannot be separated is called bound fluid. After the core fluid is separated by different centrifugal forces, we can obtain the fluid and movable fluid distributed in each pore space of the core.

The core starts to separate the movable fluid from the centrifugal force of 21 psi, and a total of 6 times of

Table 2: Statistics of fluids controlled by the throat interval in the core.

Core			The size of the fluid space controlled by the throat interval			The percentage of movable fluid controlled by the throat interval			
Core no.	Well no.	Permeability (mD)	<0.1 μm	0.1 μm-1.0 μm	>1.0 μm	0.05-0.1 μm	0.1-0.5 μm	0.5-1.0 μm	>1.0 μm
16-1	Wu 37	0.044	82.36	15.17	2.48	19.65	14.33	0.84	2.48
11-2	Wu 34	0.056	85.99	12.39	1.62	16.94	12.00	0.39	1.62
16-2	Wu 37	0.058	84.34	14.32	1.34	15.62	13.07	1.25	1.34
Average value of the permeability is less than 0.1 mD			84.23	13.96	1.81	17.40	13.13	0.83	1.81
19-1	Wu 40	0.182	58.44	38.63	2.94	8.00	23.62	15.01	2.94
13-3	Wu 37	0.570	41.37	48.81	9.82	7.04	30.45	18.36	9.82
12-1	Wu 37	0.724	43.99	48.00	8.01	8.15	31.13	16.87	8.01
19-2	Wu 40	0.909	44.45	37.97	17.58	5.36	22.52	15.45	17.58
Average value of the permeability between 0.1 and 1 mD			47.06	43.35	9.59	7.14	26.93	16.42	9.59
3-3	Wu 82	1.513	45.20	39.82	14.98	8.17	25.07	14.76	14.98
8-1	Wu 34	2.722	41.45	33.79	24.76	5.40	19.86	13.93	24.76
8-2	Wu 34	3.998	41.35	25.45	33.20	4.49	15.16	10.29	33.20
Average value of the permeability is larger than 1 mD			42.67	33.02	24.31	6.02	20.03	12.99	24.31

centrifugation are performed. According to the concern of capillary pressure and pore size, each centrifugation represents that a certain size of pore fluid is separated. By separating cores with different permeability levels, we can obtain the occurrence characteristics of fluids in the cores and the distribution characteristics of movable fluids in the cores under the condition of changing permeability.

Figure 8 shows the distribution characteristics of the core fluid. The results show that when the permeability is small, the fluid mainly exists in the nanoscale pores. As the permeability increases, the fluid in the submicron pores increases. When the permeability increases to a certain extent, the fluid distribution tends to be high on average.

The distribution of movable fluid in the core is that when the permeability is small, the movable fluid is mainly distributed in the nanopore space (Figure 9). The size of the fluid space controlled by the throat interval and the percentage of movable fluid controlled by the throat interval are shown in Table 2.

It can be seen from Table 2 that when the permeability is less than 0.1 mD, 84.23% of the fluid is distributed in the space controlled by the throat less than 0.1 μm. This type of fluid belongs to the bound fluid which is difficult to produce. For rock samples with a permeability range of 0.1-1.0 mD, 47.06% of the fluids are bound fluids, 43.35% of the fluids are present in the range controlled by the throat of 0.1-1.0 μm, and 9.59% of the fluids are present in the fluids larger than 1.0 μm. Within the interval controlled by the throat, such reservoirs have certain development potential. For rock samples with permeability greater than 1.0 mD, 42.67% of the fluids are difficult to produce, 33.02% of the fluids are present in the range controlled by the throat of 0.1-1.0 μm, and 24.31% of the fluids are present in the range controlled by the throats greater than 1.0 μm. Within the interval, such reservoirs are easier to produce and have great development potential.

4. Conclusion

(1) The study shows that the reservoirs with permeability of 0.076 mD in the study area are mainly microthroat, which is difficult to be developed by water injection. The reservoir with a certain development potential can be used as the target of water injection. The reservoir with a permeability of 2.722-3.998 mD has a relatively large proportion of fine-middle throats using the water injection development method, which is not difficult to develop

(2) The NMR spectra in the Wucangpu area are dominated by single-peak and double-peak forms, indicating that there are two or more pore structure types in the reservoir. As the core permeability decreases, the high peak of the T_2 spectrum gradually shifts to the left (low value region), indicating that there is less and less movable fluid part as the permeability decreases

(3) For rock samples with permeability greater than 1.0 mD, 42.67% of the fluids are difficult to produce, 33.02% of the fluids are present in the range controlled by the 0.1-1.0 μm throat, and 24.31% of the fluids are present in the throats greater than 1.0 μm. Within the controlled interval, such reservoirs are easier to produce and have great development potential

Data Availability

Data is available on request.

Conflicts of Interest

The authors declare that they have no conflicts of interest.

Acknowledgments

The authors appreciate the support from the Shaanxi Science and Technology Overall Planning Project (2016KTCL01-12) and Yanchang Petroleum Group Science and Technology Investment Plan Project (ycsy2016ky-A-11).

References

[1] W. Yu, H. R. Lashgari, K. Wu, and K. Sepehrnoori, "CO_2 injection for enhanced oil recovery in Bakken tight oil reservoirs," *Fuel*, vol. 159, pp. 354–363, 2015.

[2] X. S. Zhang, H. J. Wang, F. Ma, X. C. Sun, Y. Zhang, and Z. H. Song, "Classification and characteristics of tight oil plays," *Petroleum Science*, vol. 13, no. 1, pp. 18–33, 2016.

[3] T. Wu, J. He, Z. Zhao, R. Yan, J. Yao, and J. He, "The study on source-reservoir characteristics of Chang8 oil formation in Huanxian-Heqi area, Ordos basin," *Unconventional Oil & Gas*, vol. 9, no. 4, pp. 46–57, 2022.

[4] S. Du, "Characteristics and the formation mechanism of the heterogeneous microfractures in the tight oil reservoir of Ordos basin, China," *Journal of Petroleum Science and Engineering*, vol. 191, article 107176, 2020.

[5] P. Zhao, Z. Wang, Z. Sun, J. Cai, and L. Wang, "Investigation on the pore structure and multifractal characteristics of tight oil reservoirs using NMR measurements: Permian Lucaogou formation in Jimusaer sag, Junggar basin," *Marine and Petroleum Geology*, vol. 86, pp. 1067–1081, 2017.

[6] L. Chen, K. Liu, S. Jiang, H. Huang, J. Tan, and L. Zuo, "Effect of adsorbed phase density on the correction of methane excess adsorption to absolute adsorption in shale," *Chemical Engineering Journal*, vol. 420, article 127678, 2021.

[7] L. Chen, Z. Jiang, Q. Liu et al., "Mechanism of shale gas occurrence: insights from comparative study on pore structures of marine and lacustrine shales," *Marine and Petroleum Geology*, vol. 104, pp. 200–216, 2019.

[8] L. Chen, L. Zuo, Z. Jiang et al., "Mechanisms of shale gas adsorption: evidence from thermodynamics and kinetics study of methane adsorption on shale," *Chemical Engineering Journal*, vol. 361, pp. 559–570, 2019.

[9] K. Liu and M. Ostadhassan, "Estimation of the permeability of rock samples obtained from the mercury intrusion method using the new fractal method," *Fractal and Fractional*, vol. 6, no. 9, p. 463, 2022.

[10] Q. Si, X. Sima, C. Zhang, S. Wang, B. Zhang, and Q. Zhu, "Research advances in tight oil and its prospect," *IOP Conference Series: Materials Science and Engineering*, vol. 592, no. 1, Article ID 012097, 2019.

[11] Z. Cao, G. Liu, H. Zhan et al., "Geological roles of the siltstones in tight oil play," *Marine and Petroleum Geology*, vol. 83, pp. 333–344, 2017.

[12] G. Liu, Y. Bai, D. Gu, Y. Lu, and D. Yang, "Determination of static and dynamic characteristics of microscopic pore-throat structure in a tight oil-bearing sandstone formation," *AAPG Bulletin*, vol. 102, no. 9, pp. 1867–1892, 2018.

[13] H. Zhang, B. Yang, K. Zheng, J. Ta, Y. Li, and H. Shao, "Characteristics and classification evaluation of Chang 61 reservoir in H154 area of Hujianshan oilfield," *Unconventional Oil & Gas*, vol. 3, pp. 23–32, 2021.

[14] C. Yu, "Pore structure characteristics and formation mechanism of Chang 8 member tight sandstone reservoir in Fuxian area," *Unconventional Oil & Gas*, vol. 1, pp. 15–25, 2021.

[15] F. Wang, K. Yang, and J. Cai, "Fractal characterization of tight oil reservoir pore structure using nuclear magnetic resonance and mercury intrusion porosimetry," *Fractals*, vol. 26, no. 2, p. 1840017, 2018.

[16] Y. Fan, H. Wang, and F. Tan, "Control of abnormal pressure to hydrocarbon migration & accumulation-a case study on the lower assemblage of Yanchang formation in the middle area of western Ordos basin," in *7th International Conference on Energy, Environment and Sustainable Development (ICEESD 2018)*, pp. 1563–1568, Shenzhen, China, 2018.

[17] J. Cui, R. Zhu, S. Li, Y. Qi, X. Shi, and Z. Mao, "Development patterns of source rocks in the depression lake basin and its influence on oil accumulation: case study of the Chang 7 member of the Triassic Yanchang formation, Ordos basin, China," *Journal of Natural Gas Geoscience*, vol. 4, no. 4, pp. 191–204, 2019.

[18] H. Wang, L. Tian, D. Gu, M. Li, X. Chai, and Y. Yang, "Method for calculating non-Darcy flow permeability in tight oil reservoir," *Transport in Porous Media*, vol. 133, no. 3, pp. 357–372, 2020.

[19] J. Gigac, M. Stankovská, and M. Fišerová, "Comparison of capillary flow porometry and mercury intrusion porosimetry in determination pore size distribution of papers," *Wood Res*, vol. 62, no. 4, pp. 587–596, 2017.

[20] J. Liu, S. Song, X. Cao et al., "Determination of full-scale pore size distribution of Gaomiaozi bentonite and its permeability prediction," *Journal of Rock Mechanics and Geotechnical Engineering*, vol. 12, no. 2, pp. 403–413, 2020.

[21] J. W. Lee, S. H. Bae, Y. T. Hsieh et al., "A bifunctional Lewis base additive for microscopic homogeneity in perovskite solar cells," *Chem*, vol. 3, no. 2, pp. 290–302, 2017.

[22] Y. Chen, D. Gao, and X. Sun, "Organic geochemistry and evaluation of the shale of Yanchang formation in Yanchang exploration area of Ordos basin," *Unconventional Oil & Gas*, vol. 1, pp. 32–37, 2020.

[23] Z. Cui and W. Sun, "Study on pore structure of tight sandstone based on high pressure mercury and nuclear magnetic resonance—take Shanxi formation and Shihezi formation in Sulige gas field as examples," *Unconventional Oil & Gas*, vol. 2, pp. 49–55, 2020.